Available online at www.sciencedirect.com
ScienceDirect
International Journal of Heat and Mass Transfer 50 (2007) 4439–4445
International Journal of HEAT and MASS TRANSFER
www.elsevier.com/locate/ijhmt

Computer simulation and experimental verification of welding in thin steel sheet containment

Anuj Chaudhri [a], Masood Parang [a,*], B.E. Nelson [b]

[a] Department of Mechanical, Aerospace and Biomedical Engineering, University of Tennessee, 101 Perkins Hall, Knoxville, TN 37919, USA
[b] Fusion Energy Division, Oak Ridge National Laboratory, Oak Ridge, TN 37831, USA

Received 11 February 2005; received in revised form 4 January 2006
Available online 15 May 2007

Abstract

Thermal analysis of welding a thin steel sheet containment can around the modular coil winding pack of a Quasi-Poloidal Stellarator was performed. Welding causes distortions and thermal stresses to develop in the coil. Damage to the conductor coil nearest to the welding region would cause distortion of magnetic field produced by it, which would disrupt working of the stellarator. Computer weld models were developed and temperature response normalized with respect to ambient temperature was plotted at predefined locations on the cross-section of the coil. This study predicted that the maximum temperatures reached were less than the insulation melt temperatures. Independent studies using data from this study predicted that there is negligible distortion and stresses in the coil after welding. Experiments were also performed which confirmed no visual damage to conductor coil nearest to the weld zone and served to validate the computational models.

1. Introduction

Thermonuclear reactions produce large amounts of energy, which could be controlled and used for constructive purposes. Plasma confinement using a toroidal magnetic field has been the main focus of most research. Stellarators have a toroidal magnetic configuration that does not require net plasma current to produce closed magnetic surfaces. The resulting plasma shape is complex, has a periodic geometry and is not axisymmetric. The Quasi-Poloidal Stellarator (QPS) is a low aspect ratio compact stellarator with a non-axisymmetric, near-poloidally symmetric magnetic configuration, being developed at The Oak Ridge National Laboratory [1]. An integral part of the QPS design is the modular coil set that produces the primary magnetic configuration. The design and fabrication of the modular coils is a major engineering challenge due to the complexity, precise geometric accuracy and high current density of the windings.

The modular coil set design uses flexible, copper cable conductor to make it easier to wind into the complex shape. The copper cable is insulated using a nylon cloth and alternate layers of glass cloth and Kapton®. A tee-shaped structural member supports the copper cable conductors. Stainless steel sheets are welded to the tee steel member to completely enclose the windings (see Fig. 1). After enclosing the cable, it is vacuum pressure impregnated with epoxy using a prototypical impregnation and curing cycle to form a monolithic copper–glass–epoxy composite [2].

The welding process required in the containment of the conductor prior to the imposition of vacuum pressure impregnation (VPI) has important features and problems with respect to damage to conductor and residual stresses associated with it [3]. In particular the proximity of welding area to the copper and its insulation wrapping during the welding process, poses a challenge to prevent damage to the windings. In addition high local heat flux and temperature generated during welding can easily cause undesirable deflections and thermal stresses within the winding.

* Corresponding author. Tel.: +1 865 974 2454; fax: +1 865 9749879.
E-mail address: mparang@utk.edu (M. Parang).

0017-9310/$ - see front matter © 2006 Elsevier Ltd. All rights reserved.
doi:10.1016/j.ijheatmasstransfer.2006.02.052

Nomenclature

F_{1-2}	shape factor
g	acceleration due to gravity
h	convection parameter
I	welding current
k	thermal conductivity
L	length
Nu_L	Nusselt number
Pr	Prandtl number
$q(r)$	welding heat flux
q	heat flux
Q	amount of heat input
r	effective radius over which heat flux is applied
$\bar{r}$	characteristic radial dimensional distribution parameter for welding
Ra_L	Rayleigh number
T	dimensional temperature
T_{in}	ambient temperature, 297.15 K
T_1	temperature at first-thermocouple location (Figs. 4–8)
T_2	temperature at second-thermocouple location (Figs. 4–8)
T_3	temperature at third-thermocouple location (Figs. 4–8)
T_{1e}	temperature at first-thermocouple location obtained during experiment (Fig. 8)
T_{2e}	temperature at second-thermocouple location obtained during experiment (Fig. 8)
T_{3e}	temperature at third-thermocouple location obtained during experiment (Fig. 8)
T_∞	reference temperature, 300 K
T_{avg}	average temperature of surface
T_f	film temperature
V	arc voltage
x	x-axis dimension of weld area
y	y-axis dimension of weld area

Greek symbols

α	thermal diffusivity
β	$1/T_f$
ε	emissivity
η	efficiency
π	pi
σ	Stefan Boltzmann's constant
υ	kinematic viscosity

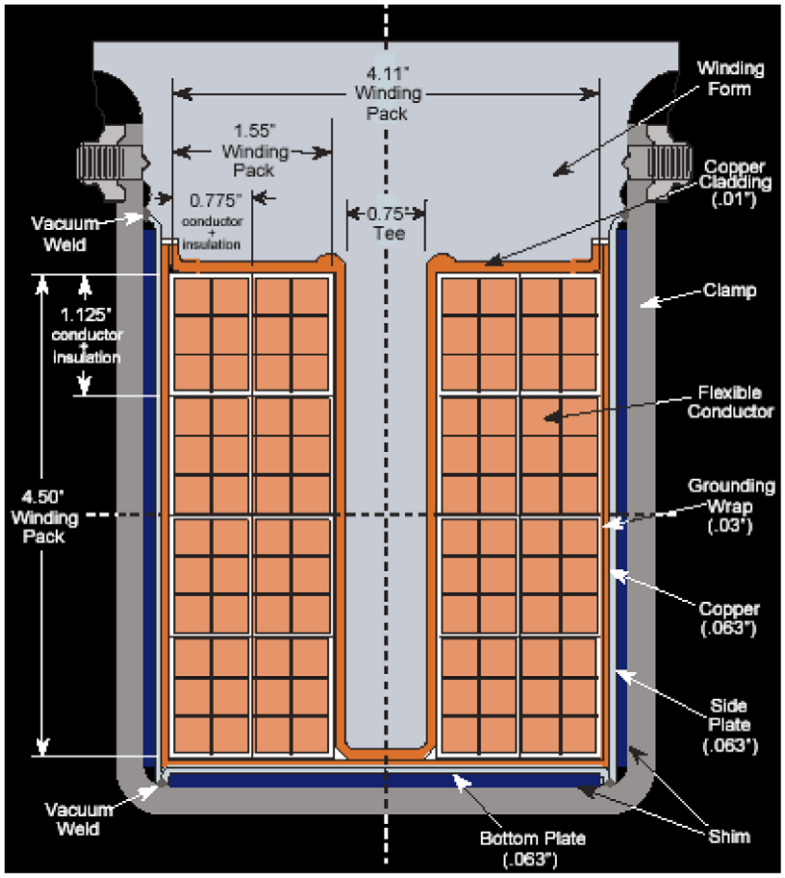

Fig. 1. Modular coil cross-section.

The problems associated with welding and their resolution were the focus of this study. For this purpose simulations of the welding process were completed using a finite element analysis with appropriate transient boundary conditions developed for this purpose. The computer simulation was verified using welding experiments in which temperature data were collected. Visual observations of the cable and its insulation were also used to assess the damage to the winding after completion of the welding process.

2. Computational model

During welding, the thermal cycles produced by the moving heat source cause metallurgical change, transient stress, and metal movement, which often results in the creation of residual stress and distortion in the finished product. The cooling cycle will also cause defects due to rapid weld solidification. To analyze these problems, it is essential to understand thermal behavior through computer simulation [4]. A set of temporal boundary condition consisting of a transient heat flux and a constant-temperature condition was developed. Finite element analysis was then carried out by incorporating the developed unsteady boundary condition in FEMLAB®. The welding problem of interest focused on a thin steel sheet (length of 4 in. and thickness of 0.06 in.). Heat transfer across the thin sheet dominates the other dimensions by two orders of magnitude. Simple numerical experiments in three dimensions also show that heat diffusion in the normal direction is the principle direction of heat transfer and computed temperature differences between the two models are within 2%. As a result it was possible to simulate the welding by a 2D model. Moreover, since a critical parameter of interest is computation of the maximum temperature along the weld line, a two-dimensional model provides a desirable upper bound and a conservative estimate of this critical quantity of interest [5].

To effectively model the entire process, latent heat of melting has to be added once melt temperature is reached. The latent heat of steel is approximately 336 kJ/kg. This addition of heat would cause a temperature rise of around 700 °C, which has been incorporated by the constant temperature boundary condition in welding the can at the top of the 'tee' section. It is believed that using a constant temperature model will not increase the uncertainty in the numerical scheme when compared with a model with phase change.

2.1. Model and properties

A computational model was developed for the welding of a thin sheet to a block of steel. It is expected that the highest temperature and outer insulation discoloration is observed in this case. The model is shown in Fig. 2. This model was later modified by adding more insulation layers between the conductor and the steel can. The containment can, which is 0.04 in. thick, was welded at two places as shown in Fig. 3. This model has only half of the symmetric conductor array. It was assumed that the heat transfer is two dimensional as in the previous case. The AISI 316 stainless steel sheet experiences significant temperature change. As a result, temperature dependent properties were considered for AISI 316 stainless steel used in the model. Copper conductors and insulation layers did not undergo large change in temperature and property data used for these layers were selected to be constant and at 300 K. For the insulation layers, property data were not available. The data used in the computational model had to be based

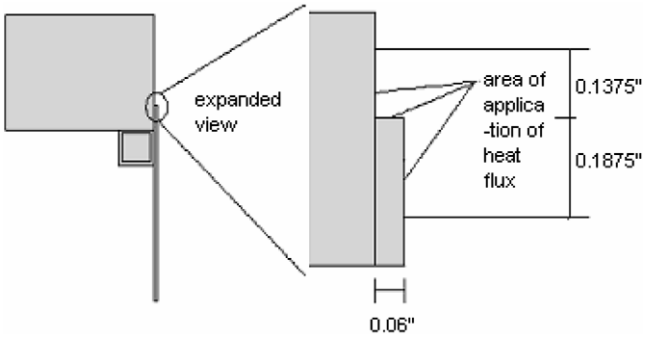

Fig. 2. Expanded view of weld area.

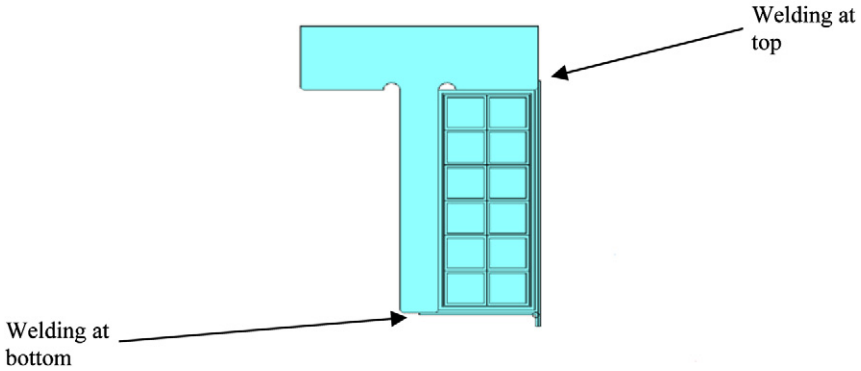

Fig. 3. Model for welding of containment can.

on the results obtained in direct measurement from simple experiments developed for this purpose.

2.2. Boundary conditions

Various boundary conditions have been tried to model the flux at the welding zone and the resulting computed temperature results were compared with the experiment. A convenient model for the weld flux boundary condition is a combined transient Gaussian heat flux followed by a constant (melt) temperature application. In this model the heat flux was applied for 0.01 s followed by 1.5 s of constant (melt) temperature. This was followed by 60 s of natural convection cooling. The basic input parameters required for thermal analysis of a weld are the magnitude of the heat input from the welding arc, the distribution of that heat on the surface of the weldment, and the weld speed. The magnitude of heat input is given by

$$Q = \eta VI \tag{1}$$

where η is the arc efficiency, V is the arc voltage and I is the current.

Following the approach from [5], the heat from the arc is, at a given time deposited on the weldment surface as a radially symmetric normal distribution function. The heat flux $q(r)$ acting on the surface is defined by the following equation:

$$q(r) = \frac{3Q}{\pi \bar{r}^2} \exp\left[-3\left(\frac{r^2}{\bar{r}^2}\right)\right] \tag{2}$$

r is the distance from the centre and $\bar{r}$ is a characteristic radial dimensional distribution parameter that defines the region in which 95% of the heat flux is deposited. In this study, η is selected as 0.5 [5]. Experimental observations show that $r = 3/16$ in. r^2 is the effective area over which the heat flux is applied, and is given by

$$r^2 = x^2 + y^2 \tag{3}$$

where x, y are the Cartesian coordinates in the weld zone.

All the surfaces are subjected to convective boundary conditions. The correlations for natural convection over a vertical plate and horizontal plate (upper or lower surface heated) were selected from [6] to calculate the heat transfer coefficients. Radiation boundary condition is applied at the weld zone where the temperature is significantly higher than the initial conditions. For natural convection over a vertical plate, the Rayleigh and Nusselt numbers are defined by

$$Ra_L = \frac{g\beta(T_{avg} - T_\infty)L^3}{\nu\alpha} \tag{4}$$

$$Nu_L = \frac{hL}{k} \tag{5}$$

All properties of air are calculated at

$$T_f = \frac{T_{avg} + T_\infty}{2} \tag{6}$$

For surfaces away from the weld zone the average temperatures do not rise much above the initial values, hence properties of air are calculated at 300 K.

The Nusselt number for natural convection over a vertical plate can be calculated as

$$Nu_L = \left\{ 0.825 + \frac{0.387 Ra_L^{1/6}}{\left[1 + \left(\frac{0.492}{Pr}\right)^{9/16}\right]^{8/27}} \right\}^2 \tag{7}$$

For natural convection over a horizontal plate with upper surface heated the Nusselt number can be calculated as

$$Nu_L = 0.54 Ra_L^{1/4} \tag{8}$$

For natural convection over a horizontal plate with lower surface heated the Nusselt number can be calculated as

$$Nu_L = 0.27 Ra_L^{1/4} \tag{9}$$

The heat transfer coefficient can then be calculated as a function of temperature of surface and initial temperature from Eq. (5). Radiation boundary condition is calculated from the following expression:

$$q = \varepsilon\sigma F_{1-2}(T_{avg}^4 - T_\infty^4) \tag{10}$$

where $\varepsilon = 0.28$ for steel and $\sigma = 5.67051 \times 10^{-8}$ W/m^2 K^4 [7].

3. Experiments

Parameters such as weld speed, weld radius (effective area of heat flux application), temperature data with respect to time, and welding power input were measured from the experiments. The damage to the conductor during and after the welding was examined visually. Thermocouples were used at predefined locations to record maximum temperature rise away from the weld zone. These locations were selected so that they could serve to validate the computational model. More details of experimental procedure beyond that described in the following sections can be found in Ref. [3]. The uncertainty in the temperature measurements in these experiments was 4%. All temperatures are normalized with respect to ambient temperature as

$$T' = \frac{T - T_{in}}{T_{in}} \tag{11}$$

3.1. TIG welding of two thin steel sheets

Two sheets of AISI 316 stainless steel, 0.06 in. thick were welded normal to each other with the copper conductor clamped to the corner on the opposite side of the weld. Thermocouples were used at three locations T_1, T_2 and T_3 as shown in Fig. 4. Digital thermometers recorded the temperature rise. Simultaneous DC voltage and current input to the weld electrode was recorded on video. The two sheets were welded in an L-shaped weld. The recorded temperatures and input power were then transcribed to

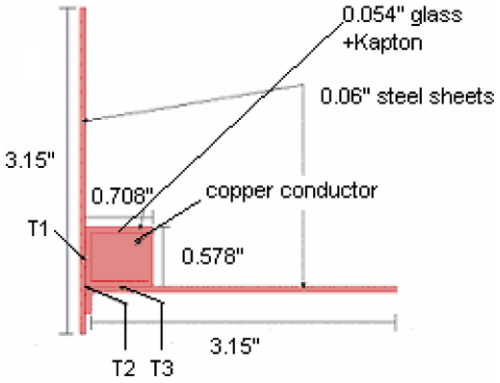

Fig. 4. Welding geometry with location of thermocouples.

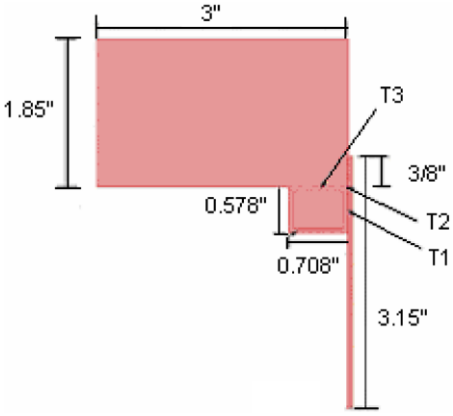

Fig. 6. Welding of thin sheet to a block of steel.

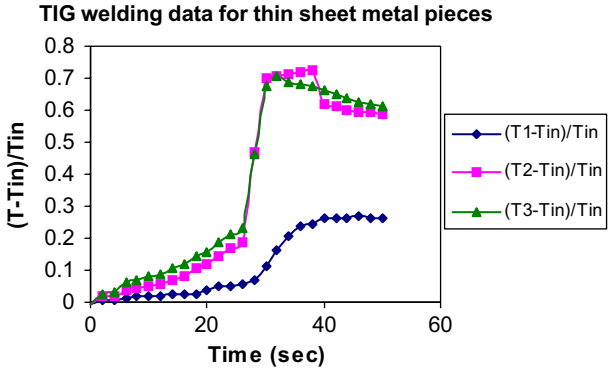

Fig. 5. Response at the thermocouple locations in Fig. 4.

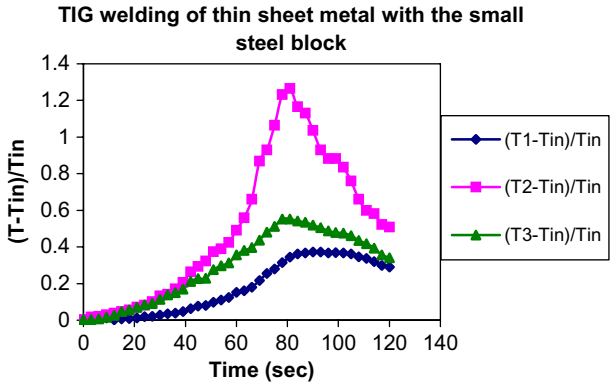

Fig. 7. Response at thermocouple locations in Fig. 6.

provide temperature as a function of time. As shown in Fig. 5, the highest temperature was recorded by the thermocouple T_2 in the corner of the L-shaped geometry as expected. Several important conclusions were made from the observations and measurements. First, there was no damage to the conductor or insulation. The glass insulation did not discolor and remained white and soft to touch. Second, maximum temperature reached anywhere on the insulation was 240 °C at T_2 and total welding time was 50 s for 2.95 in. of welding. From Fig. 5, temperature at T_1 is very low compared to T_2 and T_3.

3.2. TIG welding of thin sheet to block of steel

In this experiment a thin sheet of AISI 316 steel, 0.06 in. thick was welded to a block of steel. The copper conductor was clamped to the corner behind the weld as before. A setup similar to the previous case was used. The welding process in this case was comparatively slower as more power was needed to form the bead on the thicker block. The resultant temperatures were also higher in this case. Thermocouples were used at locations T_1, T_2 and T_3 as shown in Fig. 6. The temperature at T_2 (see Fig. 7) was as high as 400 °C.

While no damage was observed either by the conductor or insulation, there was slight discoloration of the outer layer of insulation. The total welding time was 120 s for a welding length of 4 in.

4. Results and discussion

The results from computer models are compared with experiments for validation. For model in Fig. 2 the results were compared with the experiments in Fig. 7 and are presented in Fig. 8. The computational model overestimates the temperatures at T_1 and T_3 by about 15%. These differences are expected because the model is 2D and the heat transfer in the third direction is absent. Also the overestimate of the temperature increases with the distance away from the location of the application of the heat flux. This is also the reason that T_2 (at the corner of the conductor and closest to the location of welding) is predicted much more accurately as compared to T_1 and T_3. The time in the experimental data is measured from the location of maximum temperature observed for T_2. This makes it possible to model a 2D heat transfer match as closely as possible to a 3D experimental test.

The model in Fig. 3 is an extension of the earlier case to predict the drop in temperatures between the insulation layers. The temperature response with time is plotted at five

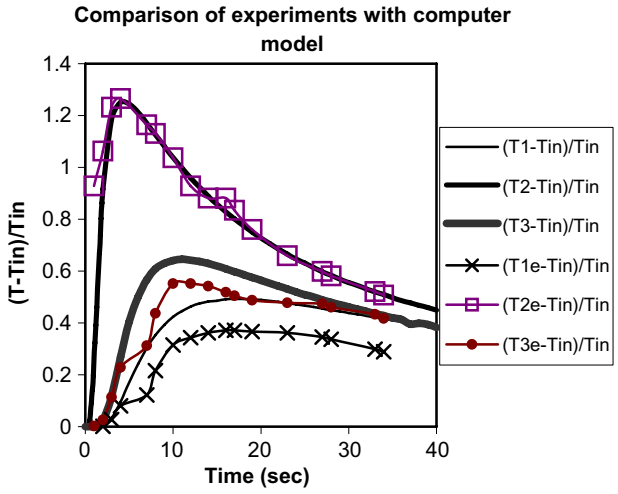

Fig. 8. Comparison of results between computational weld model and experiments.

locations at the intersection of each insulation layer for welding at top and bottom of the can. There are layers of Kapton® and glass on each conductor. The entire array is then wrapped with Kapton®, copper, and glass layers. Figs. 9 and 10 show the location and temperature response at predefined locations for welding at top of 'tee' section. The maximum temperature is directly below the edge of the steel block and the sheet and has a value of 750 °C. This temperature is smaller than glass cloth melt temperature of 820 °C. It is observed from Fig. 10 that the drop in temperatures with increase in insulation layers is significant. As discussed earlier the temperatures calculated here are expected to be conservative and upper limits for temperatures in a 3D model.

Figs. 11 and 12 show the location and temperature response for welding at bottom of 'tee' section. The temperature at the edge of the conductor practically remains at room temperature indicating no damage to the conductor whatsoever. The maximum temperature reached was found to be 225 °C at the surface of the steel sheet in contact with the glass layer. All other temperatures are below 75 °C, indicating no damage to the glass or Kapton® layers. The temperature drop between successive insulation layers is significant and hence addition of more layers to the design would not be required.

The temperature history for both welding cases at top and bottom were provided to calculate residual stresses. In another study, the results indicated little or no distortion to the 'tee' structure. These results also matched the independent welding experiments carried out at Oak Ridge National Laboratory, which provides further confidence in the model and serves as additional validation of the model.

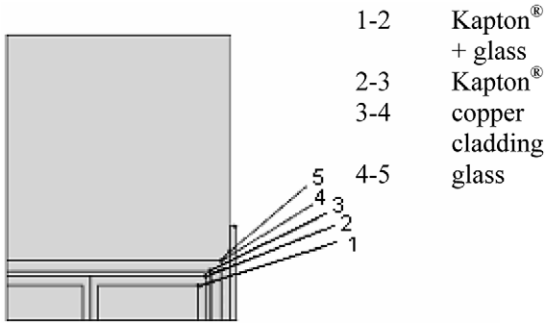

Fig. 9. Selected temperature locations at top of tee.

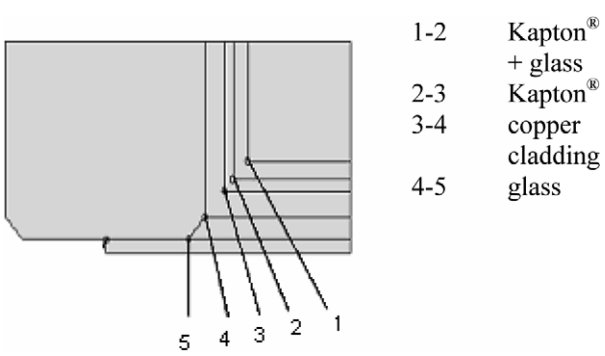

Fig. 11. Selected temperature locations at bottom of tee.

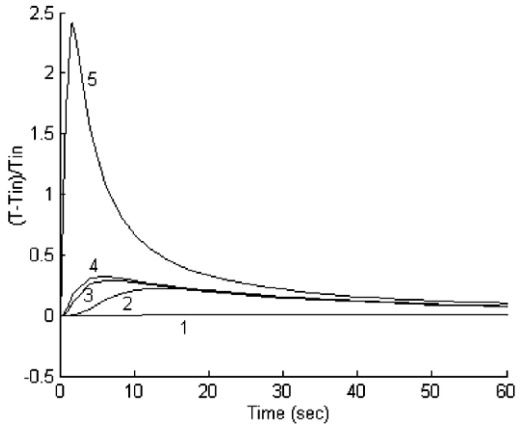

Fig. 10. Response at locations 1–5 (see Fig. 9).

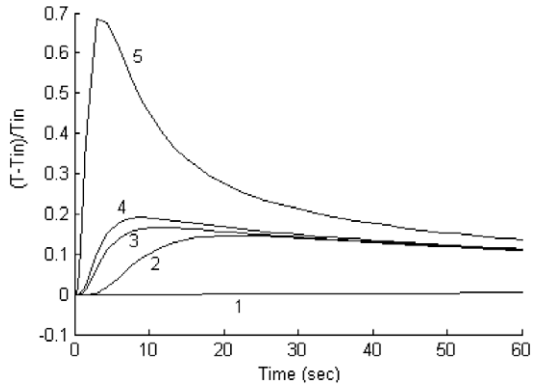

Fig. 12. Response at locations 1–5 (see Fig. 11).

5. Conclusions

The experiments validated the computational welding model and provided temperature data needed for predicting distortion of shape and residual stresses. There was no damage to the conductor or the insulation during welding of containment can. This was because the highest temperatures reached were small compared to the melting point of the insulation. A methodology using the Gaussian heat flux model developed here could serve as a useful tool for similar studies.

References

[1] B.E. Nelson et al., Design of the quasi-poloidal stellarator experiment, in: The 13th International Stellarator Workshop, February 25–March 1, Paper No. PIIB. 1, 2002.

[2] B.E. Nelson et al., Design of the quasi-poloidal stellarator experiment, in: Symposium on Fusion Technology, Helsinki, Finland, September 9–13, 2002.

[3] A. Chaudhri, Thermal Modeling and Verification of a Quasi-poloidal Stellarator Modular Coil, Master's Thesis, University of Tennessee, Knoxville, TN, August, 2004.

[4] C.L. Tsai, Heat transfer phenomena in welding processes, in: Freezing and Melting Heat Transfer in Engineering, Selected Topics on Ice–Water Systems and Casting Processes, Hemisphere Publishing Corporation, 1991 (Chapter 22), pp. 747–780.

[5] S.S. Glickstein, Basic studies of the arc welding process, Trends in Welding Research in the United States, in: Proceedings of a Conference Sponsored by the Joining Division of American Society for Metals, New Orleans, 16–18 November, 1981, pp. 3–51.

[6] F.P. Incropera, D.P. Dewitt, Fundamentals of Heat and Mass Transfer, fourth ed., John Wiley and Sons, 1996.

[7] R. Siegel, J.R. Howell, Thermal Radiation Heat Transfer, third ed., Taylor & Francis Publishers, 1992.